J Coast Conserv (2017) 21:381–392
DOI 10.1007/s11852-017-0516-6

Two and three-dimensional shoreline behaviour at a MESO-MACROTIDAL barred beach

Donatus Bapentire Angnuureng[1] · **Rafael Almar**[2] · **Nadia Senechal**[3] · **Bruno Castelle**[3] · **Kwasi Appeaning Addo**[4] · **Vincent Marieu**[3] · **Roshanka Ranasinghe**[5,6,7]

Received: 14 October 2016 / Revised: 8 February 2017 / Accepted: 19 April 2017 / Published online: 28 April 2017

Abstract The present work investigates cross-shore shoreline migration as well as its alongshore variability (with deformation) on timescales of days to years using 6 years of time-averaged video images. The variability of the shoreline is estimated through empirical statistical methods with comprehensive reference to three scales of variability. At the meso-to macro-tidal barred Biscarrosse beach, shoreline responds in decreasing order at seasonal (winter/summer cycles, 52%), event (storms, 28%) and inter-annual scales. Whereas seasonal evolution is dominated by wave climate modulation, short-term evolution is influenced by tidal range and surf-zone sandbar characteristics. The influence of tide range and sandbars increases when timescale decreases. This is even more the case for the alongshore deformation of the shoreline which is dominated by short-term evolution. An EOF analysis reveals that the first mode of shoreline change time series is associated with cross-shore migration and explains 58% of the shoreline variability. The rest of the modes are associated to deformation which explain 42% of shoreline variability.

✉ Donatus Bapentire Angnuureng
donatus.angnuureng@ucc.edu.gh; angnuureng@yahoo.com

[1] DFAS (University of Cape Coast), Cape Coast, Ghana

[2] LEGOS (University of Paul Sabatier/CNRS/IRD/CNES), Toulouse, France

[3] EPOC (University of Bordeaux/CNRS), Bordeaux, France

[4] MAFS (University of Ghana), P. O. Box LG, 99 Accra, Ghana

[5] UNESCO-IHE, Delft, The Netherlands

[6] Harbour, Coastal and Offshore engineering, Deltares, Delft, The Netherlands

[7] Research School of Earth Sciences, The Australian National University, Canberra, Australia

Keywords Video imagery · Shoreline change · Event scale · Seasonal evolution · Sandbar · Tide · Biscarrosse beach · Aquitaine coast · EOF

Introduction

Understanding and further predicting shoreline evolution is of primary interest for coastal scientists and engineers (Ranasinghe and Stive 2009). Sandy beach morphodynamics is mostly controlled by geological (e.g. headland, sediment size) and hydrodynamic (e.g. waves, tide) settings (Stive et al. 2002). Shoreline position can be defined through a wide range of proxies (see Boak and Turner 2005), with shoreline dynamics being sensitive to the proxy used (Harley et al. 2011; Castelle et al. 2014). The upper dry beach is more impacted by extreme events than the lower beach which dynamics is generally smoother and influenced by intertidal features such as sandbars. Shoreline changes include variations in both the cross-shore (migration) and alongshore (including deformation) directions. It has been known for a long time that shoreline tends to slowly migrate seaward for low- to moderate-energy waves, including post-storm conditions, while shoreline migrates shoreward rapidly during severe storms (Yates et al. 2009; Splinter et al. 2014a). These accretive and erosive sequences are generally associated with an increase in surf-zone sandbar three-dimensionality that is sometimes mirrored at the shoreline (Wright and Short 1984; van Enckevort et al. 2004).

From observation and modelling efforts, several studies (e.g. Yates et al. 2009; Hansen and Barnard 2010; Splinter et al. 2013; Splinter et al. 2014b) showed that intermediate beaches respond predominantly at seasonal timescales rather than to individual events, with the seasonal modulation of waves being the primary driver. The beach can go through

several scales of variability, though more attention has been given to longer scales (Terwindt and Kroon 1993) due to insufficient measurements at the short-term scale. Most of the long-term data series are generated without high frequency sampling (daily to weekly or monthly). Consequently, the variability at short term scales (hours to days, storm frequency) may be important but is less known. In contrast, where intensive monitoring exists, it is usually over a short period (few days to weeks). In the meantime, video imagery (e.g. Argus, Holland et al. 1997; Holman and Haller 2013) has been successful in monitoring continuously (daily) the long-term shoreline (e.g. Plant et al. 2007; Pianca et al. 2015) and sandbar (e.g. Lippmann and Holman 1989; van Enckevort and Ruessink 2003) behaviour. One main drawback of video system is that the data is remotely sensed, which therefore involves substantial errors, essentially controlled by the camera station set-up (e.g. implementation, rectification) and environment conditions (e.g sun glint, fog). Nonetheless, video monitoring provides new insight into short- to long-term beach change, which can potentially be used to drive mathematical and numerical models to further predict and investigate shoreline changes at several scales.

At barred beaches in meso-macrotidal environments, shoreline response is driven by the combined effect of sandbar and tide modulation of incoming wave energy (Masselink and Short 1993). In addition, 3D shoreline behaviour is sometimes linked to that of the offshore sandbar(s) (Castelle et al. 2010). When rip currents flow through the bay sections of crescentic sandbar, it could locally erode the beach (Sonu 1968; van de Lageweg et al. 2013). This may result from the convergence of wave energy at the shoreline because of the presence of crescentic sandbars. There could also be longshore sediment flux convergence between the shoals and the shoreline, resulting in megacusp formation. Tides and sandbar evolution have been shown to have limited impact during storms especially on meso-to-macrotidal beaches but are responsible for large variability during recovery periods (Angnuureng 2016). Noteworthy, tides and sandbar changes, as well as storms, have year-round fluctuations, which suggest their effects could be translated throughout the year. In large tidal-range environments, tide has been shown to influence the development of 3D features in the shoreline (Stokes et al. 2015), which is further addressed here for all the seasons in the year.

Historically, 2D behaviour has been quantified by statistical methods including spectral and empirical orthogonal function (EOF) methods (see Rihouey and Maron 2003; Miller and Dean 2007; Stokes et al. 2013; Lemke et al. 2014). The EOF method has commonly been used to describe shoreline spatio-temporal variability, especially at embayed or pocket beaches and constrained environments (e.g. close to breakwaters, Fairley et al. 2009; and river mouths, Pradjoko and Tanaka 2010; Blossier et al. 2015) and in the vicinity of groins (Lemke et al. 2014). Intermediate open sandy beaches often exhibit natural alongshore variability owing to the presence of rip channels. EOF modes have been used regularly to identify cross-shore profile variability but much less frequently to assess alongshore variability. The relation that EOF modes have with alongshore averaged shoreline locations (2D) and their deviations (3D) has not been studied in detail. Although EOF eigenfunctions are purely mathematical in nature they can unravel physical interpretations (Winant et al. 1975; Winant and Aubrey 1976). For instance, through bulk statistics and EOF analyses of cross shore profiles, Karunarathn et al. (2012) found that the intertidal zone is the most morphodynamically active region on a sandy beach whereas the swash zone is the most dynamic region on a mixed sand–gravel beach. Larson and Kraus (1994) used EOF to examine spatial and temporal variability of alongshore bars at Duck, North Carolina and they observed that average profile elevation change is symmetric around the mean sea level and that typical storms transport sand to nearshore.

In line with the beach variability, the relation of time series of EOF modes to the dominant beach states (dissipative/reflective and intermediate) of the Wright and Short (1984) classification is still poorly understood. Stokes et al. (2013) analysed morphodynamic changes through EOF and showed that the second most dominant mode of EOF involves the development of a periodic low-tide rip channel accompanied by a steepening of the beach and an increase in 3D structure. The authors also indicated that 40% of the beach variability was discarded as noise with respect to the EOF analysis, in contrast to Lippmann and Holman (1990) where a remaining variance was found representative of the three-dimensional morphodynamic structure. This contradiction in using EOF to explain three-dimensional changes further emphasises the need to enhance the understanding of the EOF method and its application to shoreline dataset.

The present paper aims at improving our understanding of multi-scale shoreline dynamics at a double barred meso-macrotidal beach. In Section 2, data from the 6-years of video imaging and monitoring period are presented, together with processing methods and the application of EOF. In Section 3, the results of the beach variability are accessed at three different temporal scales. Secondly, based on the EOF method, 2D and 3D are separated and the dominant time series in 2D/3D shoreline data is extracted. A discussion where the relation between the tides, sandbars and shoreline is evaluated is provided in Section 4 and concluding remarks given in Section 5.

Data and methods

Study area

Biscarrosse beach is located SW of France on the Atlantic coast (Fig. 1), and is exposed to long and energetic waves

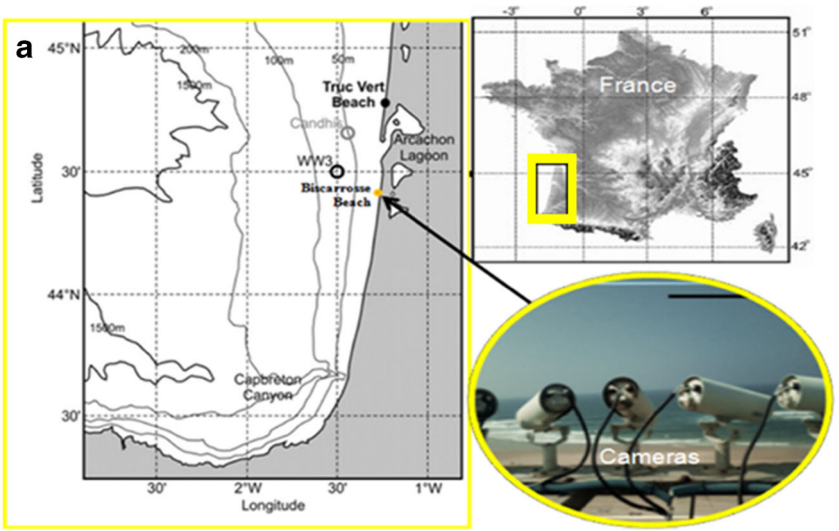

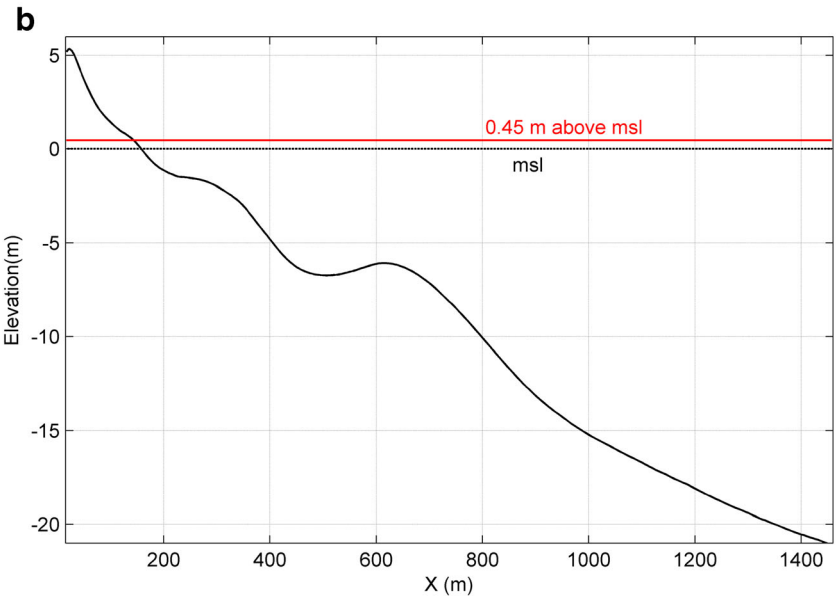

Fig. 1 **a** Location of Biscarrosse beach (SW France), with WW3 buoy located at −1°30′ W, 44°30′ N and Candhis buoy (at 1°26.8′ W, 44°39.15′ N) and video station (yellow dot on the beach). (**b**) Alongshore-averaged beach profile of Biscarrosse beach measured in June, 2007. The black horizontal line is the mean sea level while the red line is the selected water level for shoreline proxy (2.7 m above the lowest astronomical tide, i.e. 0.45 m above mean sea level)

originating mainly from the W-NW (yearly-averaged significant wave height, Hs = 1.4 m and the mean peak wave period T_p = 6.5 s). Waves reaching the Aquitanian coast are generated by W-E tracking subpolar deep low pressure systems over the North Atlantic Ocean. They are therefore, strongly seasonally modulated (Butel et al. 2002), with longer and more energetic waves in winter (November–March) and less energetic waves in summer (April – October). This meso-macrotidal beach is semidiurnal with highest and lowest tidal ranges of 5 m and 1.17 m, respectively.

Fig. 1b represents the general beach profile of Biscarrosse (Fig. 1a) which shows the presence of an inner sandbar between 200 and 400 m (Fig. 1b) and an outer sandbar around 700 m, measured during the Biscarrosse field experiment in June, 2007 (Bruneau et al. 2009). The outer bar often exhibits crescentic patterns, while the inner-bar in the intertidal domain commonly exhibits a transverse bar and rip (TBR) morphology with a mean wavelength of about 400 m (Almar et al. 2010; Peron and Senechal 2011). The average beach slope is 0.03 while sediment at the site consists of fine to medium quartz sand with sizes ranging from 0.2 to 0.4 mm (Lafon et al. 2002).

Offshore hydrodynamic forcing

The wave data are obtained from Wavewatch III model (Tolman 1991) over the 2007–2012 period at the grid point −1°30′ W, 44°30′ N facing the beach (location of the WW3 grid point is shown in Fig. 1) in about 70-m depth every 3 h. Wave height was further corrected via a linear regression fit with in situ data from a directional wave buoy (1°26.8′W,

44°39.15′ N, Fig. 1) moored at 54-m water depth (Castelle et al. 2014).

Video-derived shoreline and sandbar

A shore-based video system was installed at Biscarrosse beach in April, 2007 by the laboratory of Environments and Paleoenvironments Oceanic and Continental (EPOC) in collaboration with the New Zealand National Institute of Water and Atmosphere (NIWA). The shoreline was not visible on all parts of some images, so we selected the part (selected region on Fig. 2a) of the images where the shoreline was readily visible. The local grid origin is the camera location and the coordinate system is oriented in the cross-shore and alongshore directions. In the shoreline area, in front of the video cameras, pixel resolution is about 0.1 m and 0.2 m in the alongshore and cross-shore direction, respectively, and worsens to about 1 m and 3 m at the alongshore ends of the view field. The transformation between oblique image and real-world coordinates was achieved using 18 ground control points surveyed with a differential GPS (DGPS, centimeter accuracy) (Angnuureng 2016). The origin (X = 0, Y = 0) of the local coordinate system is the camera location oriented along the cross-shore (X) and alongshore (Y) directions while the vertical Z = 0 origin denotes the Mean Sea Level (MLS). The spatial extent of the shoreline is 600 m in the alongshore direction.

Commonly used proxies for shoreline position are either based on visual assessment (e.g. the high water line) or datum-based (see Boak and Turner 2005; Angnuureng 2016). Datum-based shorelines generally consist of the cross-shore position of a specified elevation contour, such as mean high water (MHW), the method chosen in this study. At meso- to-macrotidal barred beaches, it is difficult to select the elevation that best represents the overall intertidal complex morphology as observed by Castelle et al. (2014). Following this and to minimize the influence of the complex intertidal zone, shoreline location was defined here for elevations at 0.45 m ± 0.1 m above MSL (Fig. 2) which corresponds to the lowest high tide level, commonly used through video imagery to get daily shoreline data at meso-macrotidal beaches (e.g. Birrien et al. 2013; Senechal et al. 2015). The interface between beach and the water at this water level was manually digitized on all the images. Overall, the video-derived shoreline dataset covers 1036 days in 6 years, which is 54.2% of the study period. The high-intensity bands associated with breaking (see Fig. 2b) are commonly used as a proxy for bar crest location (Lippmann and Holman 1989; Pape and Ruessink 2008; Almar et al. 2010; Guedes et al. 2011). There is always a substantial error O (1–10 m) when locating the cross-shore position of the bar crests (van Enckevort and Ruessink 2001). This is mostly due to the translation of the breaking zone resulting from the changes in wave characteristics and tidal level (Lippmann and Holman 1989; van Enckevort and Ruessink 2001). In order to reduce the differences between the detected and actual bar crest locations, and to be consistent with previous methodologies (e.g. van de Lageweg et al. 2013; Senechal et al. 2015) images for which $Hs > 2.5$ m were discarded. Inner-bar extraction was done at a constant water level of 0.55 ± 0.1 m below MSL. All sandbar data were then manually digitized, by tracking the center of the breaking zone. The sandbar locations were extracted following existing principles (e.g. Lippmann and Holman 1989, 1990). Shoreline

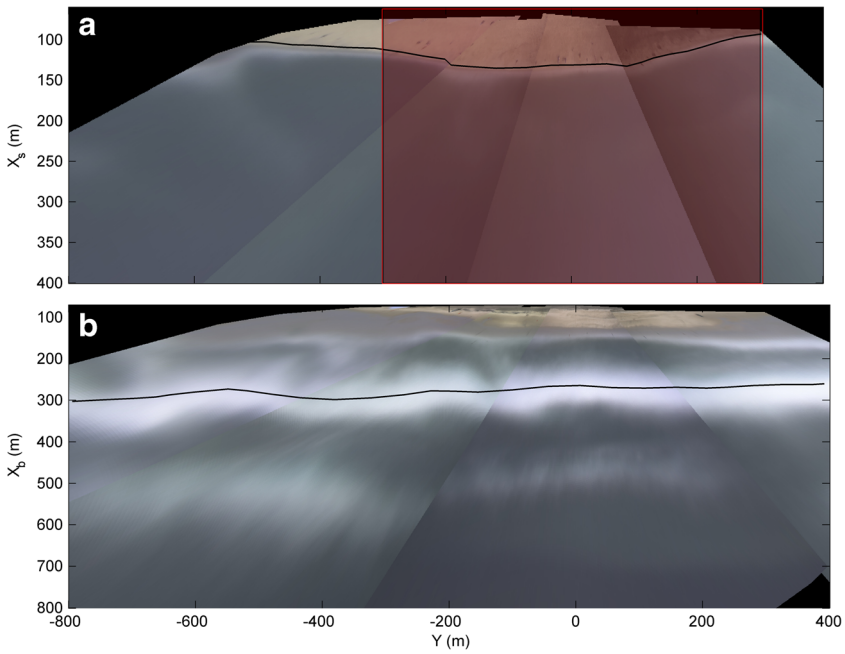

Fig. 2 Illustration of camera plan shape view field (a-d), merged and averaged over 10-min, with manual delineation of e) inner-sandbar crest (15 June, 2007) and f) shoreline (29 Sept. 2008) as black solid lines. Selected area (red box) is area of shoreline analysed

(X_s, in Fig. 2a) and sandbar (X_b, Fig. 2b) manual delineation procedure and shoreline uncertainties are extensively described in Angnuureng 2016.

In a referral, uncertainty in shoreline location is approximately ±9 m. This error margin was estimated from image rectification and shoreline digitization (Angnuureng 2016), and accounts for wave-induced set-up (an additional factor influencing the short-term nearshore water level at the scale of a storm) estimated from Stockdon et al. (2006). The uncertainty due to set-up increases when alongshore variations of set-up are large owing to large waves breaking across alongshore variable offshore sandbar(s). Tides were obtained with WXtide model (Flater 2010).

Sandbar crest location is estimated from the maximum wave dissipation proxy. The error is influenced by the water level, degree of wave breaking (e.g. Idier et al. 2011), digitisation and rectification. An average error of ±15 m was obtained.

Data processing

Based on Wright and Short (1984) classification, the beach is alongshore uniform with only variability in the cross-shore direction (2D, Fig. 3 upper plot) when it is in the dissipative or reflective state. In this regard, the shoreline shows only uniform migration. To quantify this, the alongshore-averaged cross-shore shoreline location (2D, $<X_s>$) is computed. When the beach state changes from the dissipative or reflective conditions to intermediate states, the beach becomes increasingly irregular. The beach is characterised by patterns of deformation (Fig. 3, lower plot). To account for the development of irregularities such as cuspate patterns, the shoreline alongshore non-uniformity (3D, $\sigma(X_s)$) is estimated through the alongshore standard deviation of the shoreline $\sigma(X_s)$. In this study, these two shoreline data sets (2D and 3D) are used separately.

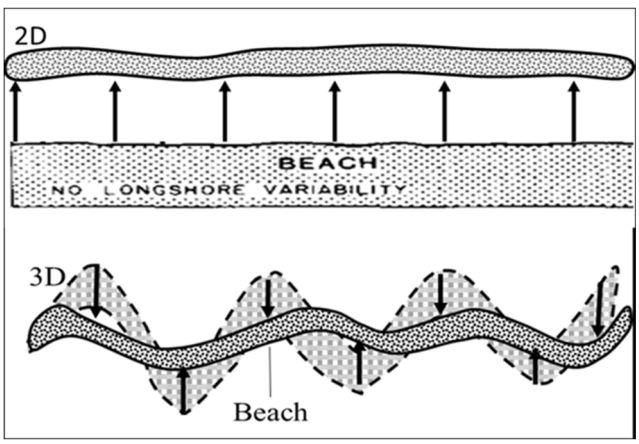

Fig. 3 Upper plot: estimating alongshore uniform migration (2D); Lower plot: estimating alongshore non-uniformiy and deformation (3D) (modified from Wright and Short, 1984)

The shoreline time series is separated into three different temporal scales; the short term (daily events, one day to one month), seasonal (monthly, one to three months) and interannual (yearly, 12 months and above) scales. For example, daily data are built by removing the neighbouring 30-day point average.

To determine the dominant scales affecting beach variability, the relative contribution $C_j(X)$ of these components to the total shoreline variability is computed as the ratio, in percentage, of the shoreline variance at each scale to the total variance (S_Y) Eq. (1):

$$C_j(X) = 100^* \sqrt{\frac{S_j}{S_Y}} (j = 1, 2, 3) \quad (1)$$

where S_j is the variance (square of the standard deviation) of daily, seasonal or interannual shoreline data and S_Y is the sum of these variances.

Empirical Orthogonal Function (EOF) analysis is widely used to investigate patterns in beach variations (e.g. Winant et al. 1975; Wijnberg and Terwindt 1995) and other coastal features (e.g. Kroon et al. 2008) compared to canonical correlation analysis (e.g. Larson et al. 2000; Karunarathn et al. 2012). In this paper, EOF analysis is implemented to obtain the uniform and non-uniform components of daily shoreline data. Singular value decomposition (SVD) is used in coastal applications as an efficient algorithm for EOF analysis (Winant et al. 1975). The SVD is applied to decompose the spatio-temporal dataset into spatial eigenfunctions $e_k(x)$, corresponding eigenvalues and associated temporal coefficients $c_k(t)$ following Miller and Dean (2007) and Lemke et al. (2014) as given by Eq. (2).

$$y(x,t) = \sum_{k=1}^{n} a_k e_k(x) c_k(t) \quad (2)$$

where $y\ (x,\ t)$ is the shoreline spatio-temporal matrix and $n = 1036$ is the number of shoreline observations; $e_k(x)$ and $c_k(t)$ are the spatial and temporal eigenfunctions, respectively. $a_k = \sqrt{\lambda_k n_x n_t}$ with λ_k the eigenvalue associated with the k^{th} eigenfunction.

In the presence of sampling variability, an ambiguity exists whenever EOFs are not well separated. The degree of separation required for uniqueness of the EOF modes depends upon the effective number of the degrees of freedom, N*, in the input data, which is equivalent to the number of independent data points in the input time series. To determine the number of EOFs to use, North et al. (1982) through the rule of thumb related the error in eigenvalues to the intervals between them. Larger intervals mean lower errors between EOFs. Indeed, if the sampling error, $\Delta\lambda = \lambda\left(\frac{2}{N^*}\right)^{1/2}$ is equal or greater than the spacing between neighbouring eigenvalues, then the errors of the associated EOFs are comparable. Determining N* is

difficult because the number of degrees of freedom in geophysical time series is difficult to estimate reliably, but space averaging can increase the effective number of independent samples and the sampling error (Leith 1973). N* was defined as $N^* = Y\left(\frac{1-r_{auto}^2}{1+r_{auto}^2}\right)$, which depends on the spatial length, Y and r_{auto}, the cumulative spatial autocorrelation divided by n. The sampling error limits the number of EOFs that can be considered significant for reconstruction of the input data. Based on these criteria, a normalized eigenvalue spectrum (not shown) of shoreline position revealed that only two modes can be considered (i.e. one significant and rest indistinguishable) to the contribution of the shoreline variability.

In contrast to Stokes et al. (2013) who use EOF to quantify the dominant modes of change occurring at monthly to seasonal time scales, therefore discarding the degenerate EOFs as noise, this study assumes that these higher or degenerate EOFs may contribute to short-term alongshore variability (see Lippmann and Holman 1990).

The next step of the analysis involved regressing changes in seasonal *TR,* sandbar locations and shoreline changes. To determine the season with predominant influence of tide or sandbar location on the shoreline, the three daily data sets were separated into winter (November to March) and summer (April to October) and cross correlated. More so, the full data sets of daily sandbar locations and tide range were also cross correlated with the shoreline positions. The influence of daily waves, cross shore energy flux and longshore flux on the individual modes were also tested by cross correlating the data and results presented.

Results

Fig. 4 shows that waves and morphological parameters follow large seasonal variations, as previously reported by Castelle et al. (2014) from bimonthly beach surveys. To eliminate any shoreline data outliers, standard z-score approach was used. This approach is used to check also how noisy the digitized data is. From the first to the last year, Fig. 4 shows that maximum summer shoreline position gradually advances seaward (at an average rate of 1.497 m/yr. from August 2007 to August 2012) suggesting an overall slow accretion over the study period. This is in line with observation in Castelle et al. (2014) at Truc Vert beach (80-km distant) who show a 4-yr. accretion trend between 2010 and 2012.

The contribution of short, seasonal and interannual scales of shoreline evolution to the total 2D (3D) variability were estimated of 28 (32)%, 52(49)% and 20(19)%, respectively (Fig. 5). Both 2D and 3D show a strong seasonality, but it is also seen in Fig. 5 that the short-term contribution is significant, though this estimation could also be influenced by noise.

Shoreline changes at daily and seasonal scales

Before daily shoreline change estimation, specious (outliers) data identified through z-score were eliminated. At the daily scale, the closest (minimum) and farthest (maximum) shoreline locations are, respectively 75 and 150 m, the average absolute 2D shoreline migration rate is 2.03 m/day (Table 1), with a maximum erosion of 11.86 m/day (24 September

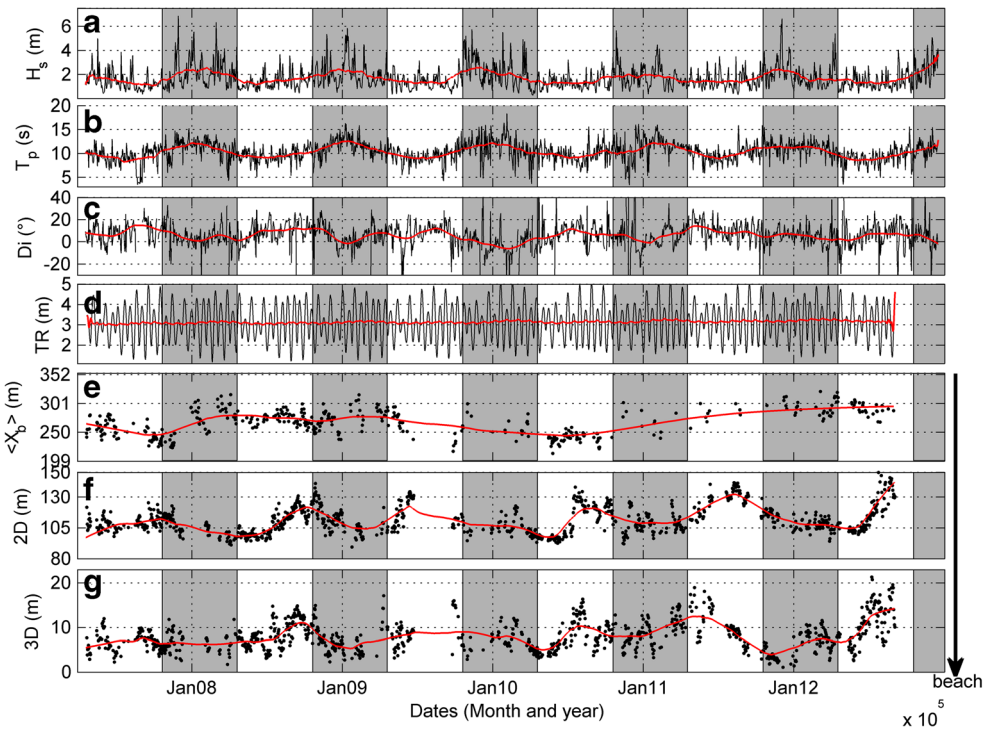

Fig. 4 Daily wave and video time series from April, 2007 to Dec., 2012; a) *Hs,* b) T_p, c) *Dir* normal to the beach, d) Tide range *TR,* e) alongshore-averaged sandbar location $<X_b>$, f) 2D $<X_s>$ and g) 3D $\sigma(X_s)$ sandbar location (black dots). Seasonal signals are shown by solid thick red lines. The location of the beach is indicated by the arrow on the morphological data

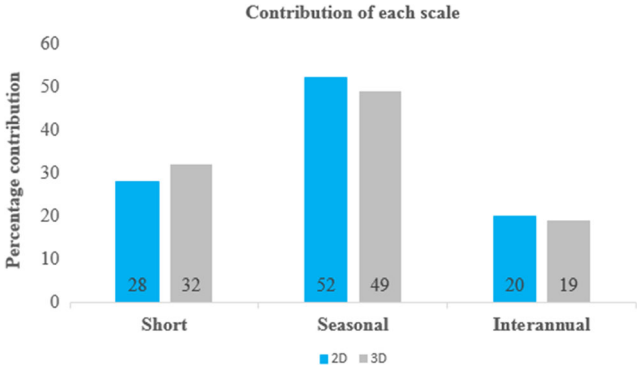

Fig. 5 The three scales of beach variability (short, seasonal and interannual scales) are estimated for both alongshore uniform (2D) and alongshore non-uniform (3D) data

2010), corresponding to the first post-summer stormy conditions. Daily sandbar location ranges from 212 to 322 m, with an average of 267 m. The extent of 3D features varies at an average rate of 1 m/day, and the maximum value is observed in summer with about 5 m/day (1st September 2012), corresponding to a summer intermediate state with the presence of a well-developed inner sandbar. The results in Table 1 suggest that daily shoreline variations may be weak in winter periods when the beach is close to an alongshore-uniform dissipative state. In general, the link between daily *Hs* and daily shoreline data is found to be weak, ($r \sim 0.35$ at zero lag, significant at the 95% level) for both 2D and 3D components. This is consistent with what has been observed at the site (e.g. Senechal et al. 2015). Wave direction shows the lowest link ($r \sim 0$) with 3D development just as T_p seems to have no influence ($r \sim 0.1$, significant at the 95% level) with 2D. These results underline that daily shoreline evolution is complex and influenced by other drivers such as tide and the presence of the sandbar, as previously observed in Angnuureng (2016). It is interesting to notice that 2D and 3D changes are weakly linked ($r \sim 0.20$) at daily scale, which suggests they can be treated separately. Nonetheless, it is important to remind that the shoreline dataset is noisy and, accordingly, that shoreline changes on short timescales is to some extent distorted.

Shoreline seasonal 2D data (Fig. 4, Table 1) show large amplitude with a wide beach in summer and fall months (+10 m from average location) while the narrowest beach is observed in spring and winter (−7 m from the average location, *see* Table 1). This is associated with a typical large accretion during the spring months (+7 m/month) and a moderate erosion (−4 m/month) during the fall months. Shoreline seasonal 3D values are largest (9 m) in spring and summer months, in consistence with Senechal et al. (2015). At the seasonal scale, the influence of seasonal *Hs* on 2D and 3D changes is moderate ($r \sim 0.3$, Table 2), yet low.

Separating 2D and 3D dynamics through EOF

The first 4 EOF components explain over 91% of the total shoreline variability distributed as 58.3, 15.6, 11.3 and 6% respectively. Based on the method described in Section 2.2, the degrees of freedom N^* is 9 while the spacing between neighbouring eigenvalues $\Delta\lambda$ is found to be larger than the difference between eigenvalues of the second and higher EOFs. This means only one distinct eigenvalue (i.e. the first) is significant while the others (referred to as the second) are indistinguishable and must be treated as one in contrast to Stokes et al. (2013) where higher modes were discarded. Thus, only two dominant time series, the first and the combined following EOF modes, are analysed. The strongest correlation ($r \sim 0.85$) is obtained between the first mode $c_1(t)$ and 2D data which is not the case for the second mode $c_2(t)$ ($r \sim -0.3$) and 2D, that is preferentially linked to 3D data (Table 3).

In Fig. 6, the temporal and spatial modes as well as the 2D/3D shorelines are compared. The second EOF spatial mode $e_2(y)$ in Fig. 6d shows opposite signs and fluctuations with nodes and antinodes at typical length of 300 m, which is not observed in $e_1(x)$. This indicates a deformation of the shoreline: extrema identify areas of maximum variability, while nodal points indicate stability (see Miller and Dean 2007). This further confirms the close link between the second EOF mode and the 3D shoreline behaviour. This also suggests the

Table 1 Alongshore uniform, 2D ($<X>$) and alongshore non-uniform, 3D ($\sigma(X)$) shoreline statistics at the daily and monthly scales relative to the mean shoreline location (105.5 m) averaged for DJF: winter, MAM: spring, JJA: summer, and SON: fall

Daily scale	*2D* (m)	Absolute Δ *(2D)* (m/day)	*3D* (m)	Absolute $\Delta(3D)$ (m/day)
Winter (Dec.- Feb)	−7	1.8	6.5	0.0
Spring (Mar. – May)	−10	2.3	8.6	1.0
Summer (Jun. – Aug.)	+6	2.6	9.6	1.5
Fall (Sep. – Nov.)	+11	2.8	8.3	1.0
Monthly scale	*2D* (m)	Absolute $\Delta(2D)$ (m/month)	*3D* (m)	Absolute $\Delta(3D)$ (m/month)
Winter (Dec. - Feb.)	−11	6.0	6.0	3.0
Spring (Mar. – May)	−7	13.0	8.6	5.0
Summer (Jun. – Aug.)	+4	11.0	9.6	4.6
Fall (Sep. – Nov.)	+10	10.0	8.0	3.0

Table 2 Correlation *r* at zero lags between wave parameters and 2D/3D data averaged over daily and monthly values, for daily and seasonal periods as indicated

	Daily correlations		Seasonal correlations	
	2D	3D	2D	3D
Hs (m)	−0.28	−0.35	−0.27	−0.32
Tp (s)	−0.07	−0.10	−0.35	−0.25
Dir (/°)	−0.13	−0.08	0.06	0.21

second EOF mode could describe the intermediate states, according to the Wright and Short (1984) classification. In Fig. 6b of $e_1(x)$, there is no node or antinode, which indicates an overall migration of the shoreline at all locations, similarly with ΔX_y spatial pattern, representing an overall alongshore-uniform migration (i.e. same sign at all longhsore locations).

In Fig. 6a, it can be seen that $c_1(t)$ and *2D* time series have a predominant seasonal evolution. In contrast, the second temporal function, $c_2(t)$ and *3D* time series (Fig. 6c) are more affected by events, which can be attributed to non-uniformities development/destruction and alongshore migration of these features.

Discussion

Two-dimensional (2D) shoreline variability

Assessing the timescales of 2D and 3D shoreline changes is of great importance for stake holders to undertake coastal zone strategies. Our results show that seasonal scale is dominant (52% of total variability) and consistent with what has been previously reported by Castelle et al. (2014) who showed that the SW France beaches respond predominantly at seasonal timescales to wave modulation. On the Ocean beach, San Francisco CA(USA), Hansen and Barnard (2010) found that seasonal processes, such as sediment supply and larger-scale morphological response, dominate the position of the shoreline. They found that the effect of storm events did have a considerable impact on the shoreline, but was largely short lived as the magnitude of the seasonal cross shore movement of sediment that corresponds to seasonal scale increases and decreases in offshore wave height. Additionally, Quartel et al. (2008) found that the seasonal pattern in beach width resulted from the cross-shore sediment exchange between the supratidal and lower-intertidal part of the beach, and beach variability between successive surveys was unrelated to the day- to week-averages of the preceding offshore wave conditions partly due to the precise timing events (e.g. storm) relative to the survey moments. Though many beaches may respond seasonally due to the wave modulation at the seasonal scale, this result may not be the same at other beaches. At the steep beach Duck, North Carolina, the shoreline change at interannual frequencies dominates seasonal variability, with wave forcing influencing only 2% variance (Pianca et al. 2015). They found that wave forcing was dominated by shorter periods (weather band) though from wave forcing it would have been expected that the shoreline response should lack interannual variability.

Not resolved in this study, therefore is that shoreline change that occurs at interannual and decadal scales and long-term trend could be of substantial importance (e.g. Pianca et al. 2015), that deserves further explanations. However, they are difficult to understand due to the lack of long-term observations and to predict because of other factors such as sea level variations (Cazenave and Nerem 2004) and sediment availability, though these longer-term rates are likely to be substantially lower (Sonu 1968; van Enckevort et al. 2004).

In this study, shoreline change due to daily events was observed, accounting for about 28% of shoreline variability. The short-term change (e.g. the storm-driven) in the shoreline, while considerably smaller in magnitude than the seasonal scale changes, provide insight into the relative timescales of beach response. However, this percentage also encompasses a large amount of noise (~15 m) in the shoreline detection method.

Table 3 Daily correlation between reconstructed shorelines of the first and second EOF functions with 2D $<X_s>$ and 3D $\sigma(X_s)$ data. $c_k(t)$ are the temporal EOF functions

Function	$<X_s>$	$\sigma(X_s)$
$c_1(t)$	0.85	0.44
$c_2(t)$	−0.32	−0.30

Three-dimensional (3D) shoreline variability

Shoreline changes in the same environmental setting have been investigated using EOF analysis. The shorelines were manually extracted from time averaged video images. In this study, results of the EOF produced well the pattern of alongshore uniform and non-uniform shoreline evolution. As suggested by Stokes et al. (2015), this EOF technique could result in a powerful tool for coastal managers to investigate coastal vulnerability and enhance shoreline prediction ability. Such empirical parametrical tools are important in predicting beach morphological state (van de Lageweg et al. 2013), and in particular, dune toe erosion during major storms for barred beaches (Sonu 1968; van de Lageweg et al. 2013; Castelle et al. 2015). Our EOF results indicate that this open beach shoreline shows both mode 1 (2D) dominated by seasonal scale and mode 2 (3D) dominated by event scale. Correlations between nearshore wave energy fluxes, wave

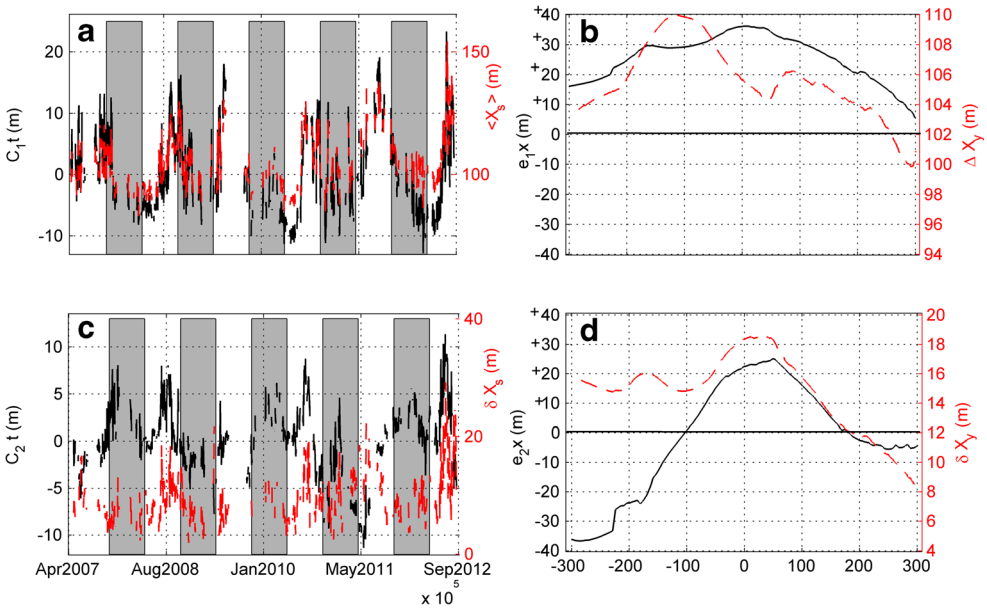

Fig. 6 EOFs (a) First temporal eigenfunction ($c_1(t)$, *black*) of shoreline variability compared to 2D $<X_s>$ (red dash line); (b) first spatial functions ($e_1(x)$, thin solid line) compared to ΔX_y (dash line); (c) second temporal eigenfunction ($c_2(t)$, black) compared to 3D $\sigma(X_s)$ (red dash line) and, (d) second spatial function ($e_2(x)$, solid line) compared to cross shore standard deviations (δX_y, dash line). The horizontal line represents the zero-crossing line that will signal deformation or migration

heights and the two EOF modes were low though significant ($p \sim 0$). The results of the correlation analysis suggest that, short-term variations in the local wave do not play the primary role in controlling the shoreline changes. Mode 1 varies at the wave modulation, which emphasizes the importance of incorporating wave conditions in the description of local morphological conditions (Angnuureng 2016). At North Beach, WA, Miller and Dean (2007) observed significant but low correlation between wave energy, cross shore flux and the principal modes (1 and 2) of shoreline change. While weak correlations may not confirm the physical impact of the derived modes, the significance ($p < 0.05$) adds confidence to these physical interpretations; they help to identify the types of nearshore conditions responsible for each individual mode of shoreline response.

However, applying EOF methods on the evolution of a beach nourishment project constructed in Long Branch, NJ, Lemke et al. (2014) found that mode 1 illustrates variations of the beach material in the direction of the net littoral drift (event scale), where several shore-perpendicular structures intercepted it while mode 2 was related to seasonal impacts. Their results suggest that the beach variation could be predominantly influenced by short term events (e.g. storms, rib currents) which further stresses the importance of the short-term scale of variation. Including 3D shoreline changes for intermediate TBR beaches such as Biscarrosse in analyses is fundamental, as they are presumably enforced by the presence of this complex submerged morphology (Bruneau et al. 2009). Unfortunately, the EOF method could not be applied to the sandbar data because only 20% of the monitoring period was available but further work could look at the coupling between shoreline and sandbar through this EOF technique to investigate coupled spatio-temporal modes (e.g. Yuhi et al. 2016). Yuhi et al. (2016) conducted an EOF analysis to capture the principal modes of systematic bar migration. They found that EOF analysis revealed that when a new bar is generated near the shoreline and a triple bar configuration is established, the shoreline tends to temporarily retreat, whereas the shoreline experiences an advance when the outer bar has most evolved.

An aspect that would certainly deserve more attention is the importance of the alongshore wavelength of the shoreline and sandbar. A great part of the shoreline 3D changes which depend on the alongshore distance is due to the alongshore migration of morphological features (Thornton et al. 2007), but were not addressed here. At this study area, the inner bar in the intertidal domain commonly exhibits a TBR morphology (Peron and Senechal 2011) with a mean alongshore averaged wavelength of about 300–400 m with a mean alongshore migration rate of about 2–3 m/day (reported at nearby Truc Vert beach, see Lafon et al. 2002; De Melo et al. 2002). Changes at $-50 < Y < 100$ m in Fig. 6d suggest the influence of rip channels. Interestingly, this goes against the fact that rip channels migrate downdrift with no preferred spatial occurrence over the years. There is a sea wall located to the right hand side of the study area though not captured on Fig. 2. The variation at this position (Fig. 6d) maybe due to the end of the seawall or break water (further north) located at the right hand side of the beach which has the potential to influence the short-term changes (Tait and Griggs 1991). Another ongoing monitoring using GPS beach survey seems to suggest that a rip is persisting but the data is under progress, and no conclusions can be given at this stage. However, the 600 m of shoreline covered in the alongshore direction of this study is somehow limiting to analysing these features and their migration. This is even truer regarding the larger scale of the outer crescentic bar that exhibit here wavelengths around 700 m at Biscarrosse

beach Almar et al. (2009) and the nearby Truc Vert beach (Castelle et al. 2007).

Effect of tides and sandbar

Coco et al. (2014) stated that the extreme *Hs* coinciding with spring tide (low tide range, *TR*) leads to the largest measured erosive events, which is what we observed here. Davidson and Turner (2009) found that a rise in *TR* can cause the sandbar to decrease in amplitude thus reducing the impact on shoreline erosion. Obviously, the tide has a smoothing effect on the beach profile. They found that the impact on shoreline erosion is also lessened by increasing the tidal range, as the impact of the storm is distributed over a broader region of the profile. In summer (April to October), the data show that correlations between seasonal daily *TR* and shoreline changes is insignificant ($r^2 \sim 0$, not significant at 95%). However, winter recorded significant correlation between *TR*, *Hs* and shoreline changes ($r^2 \sim 0.2$, significant at 95%). These results support the idea that tides can modulate wave power (Davidson et al. 2008) to cause shoreline changes, but also shows that tide influence may not be significant all year around. A test of the relative tide range (*RTR*) proposed by Masselink and Short (1993) reveals a correlation ($r \sim 0.35$, significant at 95%) higher than the correlation between the *Hs* and shoreline changes at the daily scale. The effect of the wave Hydrodynamic Forcing Index (HFI, that accounts for combined influence of large TR and Hs during storms, Almar et al. 2010) showed a weak correlation, which suggests the occurrence of large tides may have negligible impact on the shoreline changes. The same analysis was performed for sandbar location. A significant negative correlation ($r = -0.4$, significant at 95%) is found between 2D sandbar and shoreline daily positions, suggesting a coupling; erosive shoreline states occurring concomitantly with offshore (deeper) position of the inner bar, in line with Sonu (1973).

Conclusions

The alongshore-averaged shoreline cross-shore migration (2D) and deformation (3D) at the meso-macrotidal barred Biscarrosse beach is investigated from a 6-year video monitoring period. 2D shoreline variability is dominated by seasonal scale (52%), short-term event scale (28%). In contrast, 3D changes are dominated by short-term changes. These percentages encompass however data noisiness (mostly in the short-term) inherent to video remote sensing data.

An EOF method applied to the shoreline data shows good skills at separating 2D and 3D distinct dynamics: the first temporal eigenfunction which accounts for 58% of shoreline variance reflects the alongshore-uniform cross-shore migration (2D). The second and higher eigenfunctions which contribute around 42% to the shoreline variance depicts the alongshore non-uniformities (3D). This indicates that the EOF method is a suited tool to describe open beach shoreline and characterise timescales and beach states in coastal management studies.

At the meso-macrotidal barred Biscarrosse beach, 2D and 3D shoreline dynamics have distinct temporal behaviours, in particular the 3D dynamics is largely determined by intertidal morphology. The combined influence of sandbar and tidal range increases at short term, which suggest to not study these morphological features in isolation but as a coupled system, and promote to include their contribution in predicting 2D and 3D shoreline changes and response to storms.

Acknowledgements The first author is co-funded by SCAC (French embassy in Ghana) and ARTS-IRD programs. Authors acknowledge the Region Aquitaine for financially supporting the installation of the video system at Biscarrosse. This research has received support from French grant through ANR COASTVAR: ANR-14-ASTR-0019. RR is supported by the AXA Research fund and the Deltares Harbour, Coastal and Offshore Engineering Research Programme *'Bouwen aan de Kust'*. BB is supported by French "Agence Nationale de la Recherche" through project CHIPO (ANR-14-ASTR-0004-01).

References

Almar R, Castelle B, Ruessink G, Senechal N, Bonneton P, Marieu V (2010) Two and three-dimensional double-sandbar system behaviour under intense wave forcing and a meso–macro tidal range. Cont Shelf Res 30(7):781–792. doi:10.1016/j.csr.2010.02.001

Almar R, Castelle B, Ruessink BG, Senechal N, Bonneton P, Marieu V (2009) High-frequency video observation of two nearby double-barred beaches under high-energy wave forcing. *J. Coast. Res*. SI 56(2):1706–1710

Angnuureng DB (2016) Shoreline response to multiscale oceanic forcing from video imagery. Dissertation, Université de Bordeaux, pp.73–95

Birrien F, Castelle B, Dailloux D, Marieu V, Rihouey D, Price TD (2013) Video observation of megacusp evolution along a high-energy engineered sandy beach: Anglet, SW France. *J. Coast. Res*. SI 65: 1727–1732

Blossier B, Bryan KR and Winter C (2015) Simple pocket beach rotation model derived from linear analysis, *Proc. the Coastal Sediments*, edited by *P. Wang*, J. D. Rosati, and J. Cheng, pp. 1-13, San Diego

Boak EH, Turner IL (2005) Shoreline definition and detection: a review. J Coast Res 21(4):688–703. doi:10.2112/03-0071.1

Bruneau N, Castelle B, Bonneton P, Pedreros R, Almar R, Bonneton N, Bretel P, Parisot J, Senechal N (2009) Field observations of an evolving rip current on a meso-macrotidal well-developed inner bar and rip morphology. Cont Shelf Res 29:1650–1662. doi:10.1016/j.csr.2009.05.005

Butel R, Dupuis H, Bonneton P (2002) Spatial variability of wave conditions on the French Aquitanian coast using in-situ data. *J. Coast. Res*. SI 36:96–108

Castelle B, Marieu V, Bujan S, Splinter KD, Robinet A, Senecha N, Ferreira S (2015) Impact of the winter 2013-2014 series of severe Western Europe storms on a double-barred sandy coast: beach and dune erosion and mega cusp embayments. Geomorphology 238: 135–148

Castelle B, Marieu V, Bujan S, Ferreira S, Parisot JP, Capo S, Senechal N, Chouzenoux T (2014) Equilibrium shoreline modelling of a high-energy meso- macrotidal multiple-barred beach. Mar Geol 347:85–94

Castelle B, Ruessink BG, Bonneton P, Marieu V, Bruneau N, Price TD (2010) Coupling mechanisms in double sandbar systems, part 1: patterns and physical explanation. Earth Surf Proc Landforms 35: 476–486. doi:10.1002/esp.1929

Castelle B, Bonneton P, Dupuis H, Senechal N (2007) Double bar beach dynamics on the high-energy meso-macrotidal French Aquitanian coast: a review. Mar Geol 245:141–159

Cazenave A, Nerem RS (2004) Present-day sea level change: observations and causes. Rev Geophys 42:RG3001. doi:10.1029/2003RG000139

Coco G, Senechal N, Rejas A, Bryan KR, Capo S, Parisot JP, Brown JA, MacMahan JHM (2014) Beach response to a sequence of extreme storms. Geomorphology 204:493–501

Davidson MA, Turner IL (2009) A behavioral template beach profile model for predicting seasonal to interannual shoreline. J Geophys Res 114:F01020. doi:10.1029/2007JF000888

Davidson MA, O'Hare TJ, George KJ (2008) Tidal modulation of incident Wave Heights: fact or fiction? J Coast Res 24(2):151–159

De Melo AD, Howa H, Dupuis H, Oggian G (2002) Morphodynamics of ridge and runnel systems during summer. *J Coastal Res* 36:222–230

Fairley I, Davidson M, Kingston K, Dolphin T, Phillips R (2009) Empirical orthogonal function analysis of shoreline changes behind two different designs of detached breakwaters. Coast Eng 56(11–12):1097–1108

Flater D (2010) *www.wXtide32.com*. Last accessed on 25/06/2016

Guedes RM, Calliari LJ, Holland KT, Plant NG, Pereira PS, Alves FNA (2011) Short-term sandbar variability based on video imagery: comparison between time–average and time–variance techniques. Mar Geol 289:122–134

Hansen JE, Barnard PL (2010) Sub-weekly to interannual variability of a high-energy shoreline. Coast Eng 57:959–972

Harley MD, Turner IL, Short AD, Ranasinghe R (2011) A reevaluation of coastal embayment rotation: the dominance of cross-shore versus alongshore sediment transport processes, Collaroy-Narrabeen beach, southeast Australia. J Geophys Res 116(F4):F04033

Holland KT, Holman RA, Lippmann TC (1997) Practical use of video imagery in neareshore oceanographic field studies. IEEE J Ocean Eng 22(1):81–92

Holman R, Haller M (2013) Remote sensing of the nearshore. Annu Rev Mar Sci 113:5–95

Idier D, Falques A, Ruessink G, Garnier R (2011) Shoreline instability under low-angle wave incidence. *J. Geophys. Res. Earth Surface,* American Geophysical Union/Wiley, 111 (F4), 12 p

Karunarathn H, Horrillo-Caraballo JM, Ranasinghe R, Short AD, Reeve DE (2012) An analysis of the cross-shore beach morphodynamics of a sandy and a composite gravel beach. Mar Geol 299–302:33–42

Kroon A, Larson M, Moller I, Yokoki H, Rozynski G, Cox J, Larroude P (2008) Statistical analysis of coastal morphological data sets over seasonal to decadal time scales. Coast Eng 55:581–600

Lafon V, Dupuis H, Howa H, Froidefond J-M (2002) Determining ridge and runnel longshore migration rate using spot imagery. Oceanol Acta 25:149–158

Larson M, Kraus NC (1994) Temporal and spatial scales of beach profile change, Duck, North Carolina. Mar Geol 117:75–94

Larson M, Capobianco M, Hanson H (2000) Relationship between beach profiles and waves at Duck, North Carolina, determined by canonical correlation analysis. Mar Geol 163:275–288

Leith CE (1973) Standard error of time-average estimates of climate means. J Applied Meteo 12:1066–1069

Lemke L, Miller JK, Gorton A, Livermont E (2014) EOF analysis of shoreline changes following an alternative beachfill within a groin field, *Proc. 34th Intern.* Conf. Coast. Eng., pp. 12

Lippmann T, Holman R (1990) The spatial and temporal variability of sand bar morphology. J Geophys Res 95:11575–11590

Lippmann TC, Holman RA (1989) Quantification of sandbar morphology: a video technique based on wave dissipation. J Geophys Res 94: 995–1011

Masselink G, Short AD (1993) The effect of tide range on beach morphodynamics and morphology: a conceptual beach model. J Coast Res 9(3):785–800

Miller JK, Dean RG (2007) Shoreline variability via empirical orthogonal function analysis: part I temporal and spatial characteristics. Coast Eng 54:111–131

North GR, Bell TL, Cahalan RF, Moeng FJ (1982) Sampling errors in the estimation of empirical orthogonal functions. Mon Weather Rev 110(7):699–7606

Pape L, Ruessink BG (2008) Multivariate analysis of nonlinearity in sandbar behavior. Nonlinear Processes Geophysics 15:145–158

Peron C, Senechal N (2011) Dynamic of a meso to macro-tidal double barred beach: inner bar response. *J. Coast. Res*. SI 64:120–124

Pianca C, Holman R, Siegle E (2015) Shoreline variability from days to decades: results of long-term video imaging. J Geophys Res Oceans 120:2159–2178. doi:10.1002/2014JC010329

Plant NG, Aarninkhof SGJ, Turner IL, Kingston KS (2007) The performance of shoreline detection models applied to video imagery. *J. Coast. Res.,* 23(3), 658–670, doi:10.2112/1551-5036(2007)23[658:TPOSDM]2.0.CO;2.

Pradjoko E, Tanaka H (2010) Aerial photograph of Sendai coast for shoreline behavior analysis*, Proc. 32nd Intern.Conf.Coast.Eng*., doi: 10.9753/icce.v32.sediment.92.

Quartel S, Kroon A, Ruessink BG (2008) Seasonal accretion and erosion patterns of amicrotidal sandy beach. Mar Geol 250(1–2):19–33. doi: 10.1016/j.margeo.2007.11.003

Ranasinghe R, Stive MJF (2009) Rising seas and retreating coastlines. Clim Chang 97:465–468. doi:10.1007/s10584-009-9593-3

Rihouey D, Maron P (2003) Empirical eigenfunction analysis of long-term bathymetric data along the beaches of Anglet. Transactions on the Built Environment 70:1743–3509

Senechal N, Coco G, Castelle B, Marieu V (2015) Storm impact on the seasonal shoreline dynamics of a meso- to macrotidal open sandy beach (Biscarrosse, France). Geomorphology 228:448–461

Sonu CJ (1973) Three-dimensional beach changes. J Geol 81:42–64

Sonu CJ (1968) Collective movement of sediment in littoral environment. J Coast Eng 24:373–400

Splinter KD, Turner IL, Davidson DA, Barnard P, Castelle B, Oltman-Shay J (2014b) A generalized equilibrium model for predicting daily to inter-annual shoreline response, *J. Geophys. Res.- Earth Surface*, 119, 1936–1958, doi:10.1002/2014JF003106.

Splinter KD, Carley JT, Golshani A, Tomlinson R (2014a) A relationship to describe the cumulative impact of storm clusters on beach erosion. Coast Eng 83:49–55

Splinter KD, Turner IL, Davisdson MA (2013) How much data is enough? The importance of morphological sampling and duration for calibration of empirical shoreline models. Coast Eng 77:14–27

Stive MJ, Aarninkhof SGJ, Hamm L, Hanson H, Larson M, Wijnberg KM, Nicholls RJ, Capobianco M (2002) Variability of shore and shoreline evolution. Coast Eng 47:211–235

Stockdon HF, Holman RA, Howd PA, Sallenger AH (2006) Empirical parameterisation of setup, swash and run up. Coast Eng 53:573–588. doi:10.1016/j.coastaleng.2005.12.005

Stokes C, Davidson M, Russell P (2015) Observation and prediction of three-dimensional morphology at a high-energy macrotidal beach. Geomorphology 243:1–13

Stokes CH, Russell P, Conley D, Beaumont E, Greaves D (2013) Exploring monthly to Seasonal Beach Morphodynamics using empirical orthogonal functions.In: Conley, D.C., Masselink, G., Russell, P.E. And O'Hare, T.J.(eds.), proceedings 12thInternational

coastal symposium (Plymouth, England), J. Coast. Res., S.I. 65, 1868-1873.

Tait JF, Griggs GB (1991) Beach response to the presence of a seawall; comparison of field observations: Contract Report CERC (http://www.dtic.mil/dtic/tr/fulltext/u2/a237709.pdf)

Terwindt JHJ, Kroon A (1993) Theoretical concepts of parameterization of coastal behavior. *U.S. Geol. Surv.* Open File Rep 93-381:193–196

Thornton EB, MacMahan JH, Sallenger AH Jr (2007) Rip currents, mega-cusps, and eroding dunes. Mar Geol 240:151–167. doi:10.1016/j.margeo.2007.02.018

Tolman HL (1991) A third generation model for wind waves on slowly varying, unsteady and inhomogeneous depths and currents. J Phys Oceanography 21:782–797

van de Lageweg WI, Bryan KR, Coco G, Ruessink BG (2013) Observation of shoreline–sandbar coupling on an embayed beach. Mar Geol 344:101–114. doi:10.1016/j.margeo.2013.07.018

van Enckevort IMJ, Ruessink BG, Coco G, Suzuki K, Turner IL, Plant NG, Holman RA (2004) Observations of nearshore crescentic sandbars. J Geophys Res 109:C06028. doi:10.1029/2003JC002214

van Enckevort IMJ, Ruessink BG (2003) Video observations of nearshore bar behaviour. Part 1: alongshore uniform variability. *Cont. Shelf Res.,* 23, 501–512, doi:10.1016/S0278-4343(02)00234-0.

van Enckevort IMJ, Ruessink BG (2001) Effect of hydrodynamics and bathymetry on video estimates of nearshore sandbar position. J Geophy Res 106(C8):16969–16979

Wijnberg KM, Terwindt JHJ (1995) Extracting decadal morphological behavior from high-resolution, long-term bathymetric surveys along the Holland coast using eigenfunction analysis. Mar Geol 126:301–330

Winant CD, Aubrey DG (1976) Stability and impulse response of empirical Eigenfunctions. *Proc. 15th International Conference on Coast. Eng*. ASCE publishing, New York, pp. 1312–1325.

Winant CD, Inman DL, Nordstron CE (1975) Description of seasonal beach changes using empirical eigenfunctions. J Geophys Res 80(15):1979–1986. doi:10.1029/JC080i015p01979

Wright LD, Short AD (1984) Morphodynamic variability of surf zones and beaches: A synthesis. Mar. Geol 56:93–118

Yates ML, Guza RT, O'Reilly WC (2009) Equilibrium shoreline response: Observations and modeling. J. Geophys. Res., 114, doi:10.1029/2009JC005359.

Yuhi M, Matsuyama M, Hayakawa K (2016) Sandbar Migration and Shoreline Change on the Chirihama Coast, Japan. J Mar Sci Eng *4*(2):40. doi:10.3390/jmse4020040